교육학 석사학위논문

Electrochemical sensing of hydrogen peroxide using Prussian Blue on poly(*p*-phenylenediamine) coated Multi-walled carbon nanotubes

파라-페닐렌다이아민이 입혀진
다중벽 탄소나노튜브에 프러시안 블루
나노복합물을 통한 과산화수소의 전기화학적 검출

2016년 2월

서울대학교 대학원
과학교육과 화학전공
전 영 은

CONTENTS

List of Schemes and Tables

List of Figures

Abstract

Electrochemical sensing of hydrogen peroxide using Prussian Blue on poly(*p*-phenylenediamine) coated Multi-walled carbon nanotubes

Youngeun Jeon
Chemistry Education Major
Department of Science Education
The Graduate School
Seoul National University

In this study, multiwalled carbon nanotubes@poly(*p*-phenylenediamine) -prussian blue (MWCNTs@P*p*PD-PB) nanocomposites were synthesized

and used for the nonenzymatic electrochemical detection of hydrogen peroxide (H_2O_2). The P*p*PD layer helps not only the MWCNTs to be dispersed in the water but also the PB to be formed and fixed. Moreover, P*p*PD, a conductive polymer, increases the electronic conductivity and stability of MWCNTs. By combining the selectivity and catalytic capacity of PB for H_2O_2, a synergistic effect was observed for the H_2O_2 detection. The morphology and chemical composition of the MWCNTs@P*p*PD-PB nanocomposites were characterized by Fourier transform infrared spectroscopy, transmission electron microscopy, and X-ray diffraction. A facile electrochemical H_2O_2 sensor based on the MWCNTs@P*p*PD-PB modifed glassy carbon electrode (GCE/MWCNTs@P*p*PD-PB) was prepared by the drop-casting method. Its electrochemical behavior was investigated using electrochemical impedence spectroscopy, cyclic voltammetry, and amperometry. The modified electrode exhibited a good electrocatalytic response for the reduction of H_2O_2 in acidic solution (pH 2.7). The proposed sensor exhibited a linear behavior in the concentration range from 0.005 mM to 2.225 mM for H_2O_2 with a high sensitivity and detection limit of 583.6 $\mu A\ mM^{-1}\ cm^{-2}$ and 0.95 μM (S/N = 3) at an applied potential of +0.15 V (vs. Ag/AgCl). The sensor showed excellent selectivity, reproducibility, and stability.

In summary, this study gives the development of these synthetic methods that are presented at the best condition for the electrochemical detection of H_2O_2, which is expected to be applied to a variety of electrochemical sensors in the subsequent studies.

Key words: Prussian blue, Poly(*p*-phenylenediamine), Multi-walled carbon nanotubes, Hydrogen peroxide, Amperometry, Sensor

Student Number **: 2014-20956**

Electrochemical sensing of hydrogen peroxide using Prussian Blue on poly(p-phenylenediamine) coated Multi-walled carbon nanotubes

1. Introduction

Prussian Blue (PB) having an open, zeolite-like structure is well known as the prototype of a number of polynuclear transition-metal hexacyanometalates with the formula, $Fe_4^{III}[Fe^{II}(CN)_6]_3$ [1,2]. It exhibits electrochemical [3-5], electrochromic [6-8], photophysical [9,10], and magnetic properties [11,12]. In particular, the electrocatalytic property among these special properties enables the potential analytical application of electrochemical sensor using the PB-modified electrode [13,14].

The reduced form of PB is prussian white (PW), which is colorless. PW can catalyze the electrochemical reduction of hydrogen peroxide (H_2O_2) at low potentials [15]. Moreover, H_2O_2 is significantly reduced excluding the interference from mixture in the presence of glucose, ascorbic acid, citric acid, dopamine, and uric acid [16,17]. Because of the peculiar structure of PB, small molecules such as H_2O_2 can penetrate into the lattice and can be reduced. However, larger molecules cannot penetrate [14]. PB not only acts as a catalyst, but also as a charge transfer mediator for H_2O_2 detection. Because of its high electrocatalytic activity and selectivity, it is usually regarded as "Artificial enzyme peroxidase" [18,19].

The first study on the synthesis of PB film was reported by Neff *et al.* [20], and various methods have been used to fabricate different PB-based hybrids for PB-modified electrode so far. Almost all the procedures adopted for the PB deposition on electrode surface are based

on electrochemical methods [21], involving a constant applied potential [22-24], or potential cycling [25,26] in a solution of ferric and ferricyanide ions. Another approach for the PB deposition is based on the chemical synthesis without the need for an electrochemical step. The chemical procedure can be performed in situ by different ways from the solutions of Fe^{2+} ions and $[Fe(CN)_6]^{3-}$ ions [27], Fe^{3+} and $[Fe(CN)_6]^{4-}$ [28,29], or from Fe^{3+} and $[Fe(CN)_6]^{3-}$ [30-32] in the presence of H_2O_2 and pre-synthesis supported on a substrate followed by the entrapment inside the bulk of composite electrodes [33]. In the former procedure that used electrochemical methods, the main disadvantages are lower solubility, difficulty of mass production, and lack of reproducibility. In contrast, using in situ chemical synthesis, PB can be homogeneously soluble in common solvents, making a uniform dispersion, thus overcoming the problems of chemical synthesis [21].

To improve the sensitivity and stability of the PB-based electrochemical sensors, several methods have been used to synthesize PB nanoparticles (PBNPs) over a range of sizes and shapes by chemical processes. For the first time, Mann *et al.* prepared PBNPs in a spatial confinement using the reverse micelles technique [34]. The synthesis of PBNPs has also been reported using ionic liquids [35,36], mesoporous silicate [37], or polymer beads [38] as mediums or templates. Despite many reported methods, developing a simple and effective synthesis of such nanoparticles and uniform particle distribution is still required.

The synthesis of PBNPs using functionalized organic polymers has been widely studied. These polymers provide the chemical and spatial

environment, allowing for the stable construction of particles. They also help to form a colloid and prevent the solution from aggregation. Using the excellent properties of the nanoparticles, potential applications in diverse fields have been attempted. Research on conductive polymers has continued owing to their excellent physicochemical properties resulting from their unique π-conjugated system [39]. These composite NPs provide a powerful platform for sensing applications and a variety of functions from the polymers.

Para-phenylenediamine (*p*PD) is one of the three isomers of phenylenediamine and has been studied worldwide. Yang *et al.* (2012) reported the polymerization of *p*PD by oxidation in an aqueous solution with ammonium persulfate (APS) as the oxidant [40]. Poly(*p*-phenylenediamine) (P*p*PD) can be formed as a polymer of a ladder-type structure such as the polyaniline chain. It is one of the most studied multifunctional polyaryldiamines owing to the characteristics of the enhanced redox activity by the presence of amino groups in the chain of P*p*PD. Moreover, it has been focused on its exceptional multifuctionality owing to various properties such as variable conductivity [41], colorful electrochromism [42], strong electroactivity [43], and high environmental and thermal stability [44].

The conductivity of P*p*PD is very low [45]. However, the use of a conductive inorganic material such as carbon nanotubes [46], noble metals [47], or nanoparticles [48] can increase the conductivity. Through this, P*p*PD can be made available to the electrolysis or the electrochemical sensors. In particular, the combination of the conductive polymer and carbon nanotubes may enable a nanocomposite with a

significantly improved electrical conductivity and thermal stability.

Single or multiwalled carbon nanotubes (MWCNTs) have been the object of constant interest based on their initial studies by Iijima *et al.* [49] and have been applied in a variety of research fields owing to their outstanding characteristics. In particular, MWCNTs, composed of π -conjugated networks, have a high electrical conductivity [50], excellent thermal stability, and large surface area, including the advantage of easily functionalization or the manipulation of their surface properties [51].

For efficient analysis, MWCNTs should be uniformly dispersed in the sample solution to form a good combination with the analytes. However, the pristine MWCNTs are not immediately dispersed in aqueous or nonaqueous solutions, because of their high hydrophobicity [52]. In order to solve this problem, two strategies for their well dispersion in the analysis solution were proposed: a method for the direct oxidation of the MWCNTs and another method of coating hydrophilic polymer in the MWCNTs. In the case of direct oxidation, many carboxyl groups are created on the MWCNTs's walls, making them hydrophilic, thus increasing the dispersion of the oxidized MWCNTs in the solution. However, the structure of the MWCNTs is destroyed in the process of direct oxidation. As a result, the oxidized MWCNTs may lose the properties of the pristine MWCNTs, that is, their high electrical conductivity and excellent thermal stability. The proposed method to reduce the destruction of the structure of the MWCNTs is by coating polymers on the surface of MWCNTs. Their original properties can be maintained as the structure of MWCNTs is

retained, and the dispersion can be increased by using hydrophilic polymers.

The analysis of H_2O_2 is of significant importance in many different fields. While H_2O_2 is commonly used as an oxidizing agent, it is a byproduct of several selective oxidases and an essential mediator in biology, food, medicine, industry, and environmental areas [52,53]. A number of methods such as chemiluminescence [54], fluorescence [55], spectrophotometry [56], and electrochemical techniques have been reported for the accurate detection of H_2O_2 concentration. The accuracy of the detection of H_2O_2 has been increased with the development of detection techniques for each area, and the electrochemical sensors in particular play more important roles. The electrochemical sensors are very useful, because they have the operational simplicity, low cost, high sensitivity, and suitability for real-time detection [57]. The studies using the redox enzyme based sensors have been conducted for the detection of H_2O_2 concentration owing to the high selectivity and specificity of H_2O_2. However, enzyme-based sensors are relatively unstable, very sensitive to environmental conditions, and expensive to prepare. As a solution to this, many researchers have conducted various studies to develop a nonenzymatic H_2O_2 electrochemical sensor utilizing inorganic materials. In particular, using the transition metal is enough to act as a nonenzymatic electrocatalyst showing thermodynamic stability, high sensitivity, and low detection limits.

In this study, for the application of electrochemical H_2O_2 sensor, the MWCNTs coated with a conductive polymer based on the PBNPs were proposed. The MWCNTs@P*p*PD was synthesized by simply coating

P*p*PD on MWCNTs and used to form the PBNPs with PB precursors in an acidic solution. By using the P*p*PD, the synthesized MWCNTs@P*p*PD-PB nanocomposites were well dispersed in aqueous solution and has the homogenous arrangement of PB on MWCNTs@P*p*PD. These composites maintained good electrical conductivity through wrapped P*p*PD on MWCNTs and formed stable PBNPs to the strong electrical catalyst for H_2O_2 by attaching PB to P*p*PD. This system displayed suitable linear range, low detection limit, and high sensitivity. In addition, it has a high selectivity to ignore the interfering species such as ascorbic acid, uric acid, and L-cysteine.

2. Experimental

2.1. Chemicals and reagents

Multi-walled carbon nanotubes (MWCNTs, 95% purity, diameter 10–15nm) were purchased from ILJIN Nanotech Co. (Korea) and used without further purification. Ammonium persulfate ($(NH_4)_2S_2O_8$, APS), *p*-phenylenediamine ($C_6H_8N_2$, *p*PD, ≥99.0%), potassium ferricyanide ($K_3Fe(CN)_6$, 99+%), potassium ferrocyanide ($K_4Fe(CN)_6$, 99%), iron(III) chloride ($FeCl_3$, 97%), potassium chloride (KCl), acetic acid (99.7 wt.% in H_2O), hydrogen peroxide (H_2O_2, 30 wt.% in H_2O), nafion (~5% in a mixture of lower aliphatic alcohols and water), ascorbic acid, uric acid, and glucose were purchased from Sigma-Aldrich Co. (USA). L-cysteine was purchased from Yakuri Pure Chemical Co. (Japan). All the chemicals were of analytical reagent grade and used without further purification. All the solutions were prepared with deionized water (DW) obtained from an ultra-pure water purification system (Human Co., Korea) with a resistivity of not less than 18.2 MΩ cm. All the measurements were carried out at room temperature.

2.2. Apparatus and measurements

The surface morphology of composites was characterized by transmission electron microscopy (TEM, Zeiss LIBRA 120, Germany).

The samples for TEM were prepared by placing a drop of the dispersion on a carbon-coated copper grid. Fourier transform infrared spectra (FTIR) were recorded using a Perkin-Elmer Spectrumv 2000 FTIR spectrometer in the range from 400 to 4000 cm^{-1} with a KBr pellet. Powder X-ray diffraction (XRD) analyses were performed using a New D8 advance diffractometer. Electrochemical impedance spectroscopy (EIS) measurements were performed using a CHI 760B electrochemical analyzer (C.H. Instrument, Inc., USA), and cyclic voltammetry (CV) and amperometry were performed using a CHI 842B electrochemical analyzer (C.H. Instrument, Inc., USA) with conventional three-electrode system. A bare or modified glassy carbon electrode (GCE, d = 3.0 mm) was used as the working electrode. A platinum (Pt) electrode served as the auxiliary electrode and a silver/silver chloride (Ag/AgCl) electrode filled with 3 M KCl was served as the reference electrode. All ultrasonic cleaning was performed using a US-2510 Ultrasonic Cleaner (Branson, USA). Before each electrochemical measurement, solutions were thoroughly deoxygenated by bubbling nitrogen through the solution for at least 10 min, to remove the dissolved oxygen.

2.3. Fabrication of MWCNTs@PpPD nanocomposites

Pristine MWCNTs (2.0 mg) were added to 17.6 mL of DW and well dispersed by a 30-min sonication. To this solution, 2.0 mL of 0.1 M *p*PD and 0.4 mL of 0.1 M APS were added at room temperature under

vigorous magnetic stirring for 24 h. The dark purple solution was carefully filtered through a membrane filter and washed thrice with double distilled water. The collected precipitate was dried overnight in an oven at 40 °C. Finally, the product was dispersed in acidic solution at pH 3.5.

2.4. Preparation of MWCNTs@PpPD-PB nanocomposites

$K_3Fe(CN)_6$ (1 mM) was added to 25 mL of 0.1 M KCl solution adjusted to pH 2.7 with acetic acid. To this solution, dispersed MWCNTs@PpPD solution (0.8 mL, 0.5 mg mL^{-1}) was added under magnetic stirring for 5 min. $FeCl_3$ (25 mL, 1 mM) was added slowly to this mixture with continuous stirring at room temperature for 1 h. Subsequently, 2 μL of H_2O_2 (30%) was added to the mixed solution. The color of this solution gradually changed from yellowish green to dark blue. After 3 h, the obtained dispersion was filtered, rinsed with double distilled water several times, and finally redispersed in 10 mL of deionized water.

2.5. Electrode modification

Before modification, the glassy carbon electrode was polished to acquire a mirror-like surface with fine alumina powders (particle size: 0.3 μm and 0.05 μm) on a polishing pad. The electrode was cleaned

and sonicated with double distilled water for 2 min, in sequence. After dried under a gentle stream of N_2 gas, the modified electrode was prepared by dropping 8 μL of the MWCNTs@P*p*PD-PB dispersion on to the purified GCE surface and dried in an oven at 40 °C for 2 h. Then, 2 μL Nafion (0.5%) was also placed on the surface of the modified electrode and it was dried again in an oven at 40 °C for 1 h.

3. Results and Discussion

3.1. Characterization of the MWCNTs@PpPD and MWCNTs@PpPD-PB nanocomposites

The synthetic route for MWCMT@P*p*PD-PB is illustrated in scheme 1. Each step of the process was synthesized by following literature procedure. At first, to synthesize the MWCNTs coated with *p*PD polymer, the pristine MWCNTs were dispersed in neutral solution through 30-min sonication. *p*PD monomer was added to the dispersion solution, and 30 s later, APS was further added resulting in a dark-violet solution. The mixture was gently stirred magnetically for 24 h to ensure that the polymerization process was conducted sufficiently. Therefore, MWCNTs were wrapped with PpPD by polymerization by π-π stacking interaction and van der Waals forces. The probable polymerization reaction can be shown in scheme 2 [58]. The precipitate from this step was redispersed in an acidic solution (pH 3.5). The snapshots of the products for each step are shown in scheme 3. The pristine MWCNTs were aggregated, but MWCNTs@P*p*PD in the neutral (Scheme 3(a)) or acid-treated solution (pH 3.5) (scheme 3(b)) was present in stable, homogeneously well dispersed state. And then, PBNPs on the modified MWCNTs were synthesized according to the reference [16]. A typical synthetic procedure was based on the reaction of $FeCl_3$ and $K_3Fe(CN)_6$. The cationic MWCNTs@P*p*PD nanocomposite was added in an acidic solution (pH 2.7) containing $K_3Fe(CN)_6$ and stirred

magnetically for 5 min. Then, $FeCl_3$ was dripped very slowly over 1 h. After that, ferricyanide anions were preattached onto that cationic surface by electrostatic attraction for stable adhesion to the surface of MWCNTs@P*p*PD. As a result, PBNPs grew well through $FeCl_3$ and H_2O_2. The formation reaction of PBNPs is expressed by the following equation [59]:

$$2Fe^{3+} + 2Fe(CN)_6^{3-} + H_2O_2 + 2K^+ \rightarrow 2KFe[Fe(CN)_6] + O_2 + 2H^+$$

The color of the dispersion changed from dark violet to yellow green initially, and while the reaction continued, the color changed to dark blue (Scheme 3(d)).

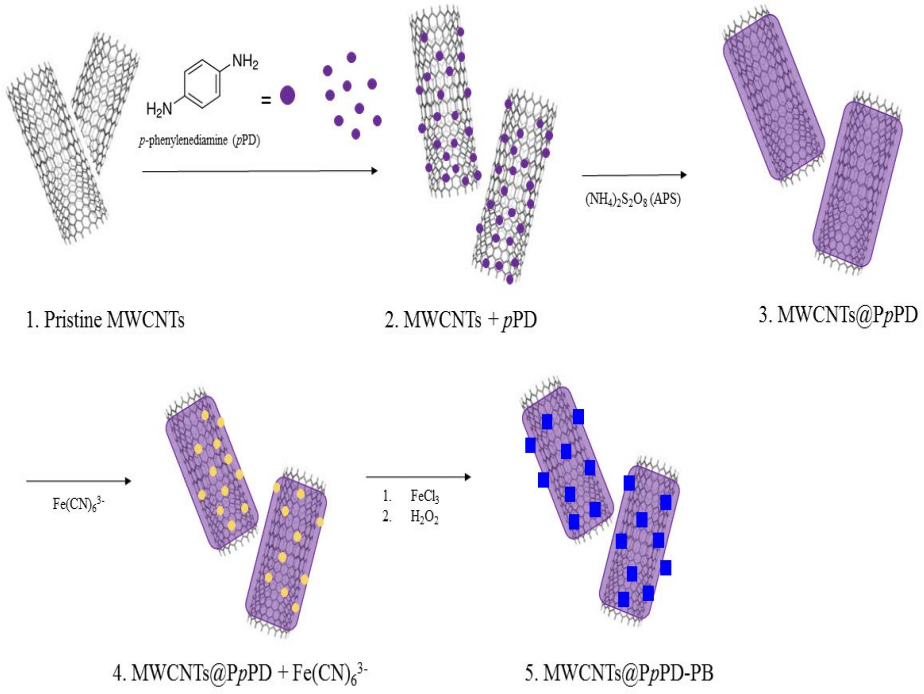

Scheme 1. Synthesis of MWCNTs@P*p*PD-PB nanocomposites.

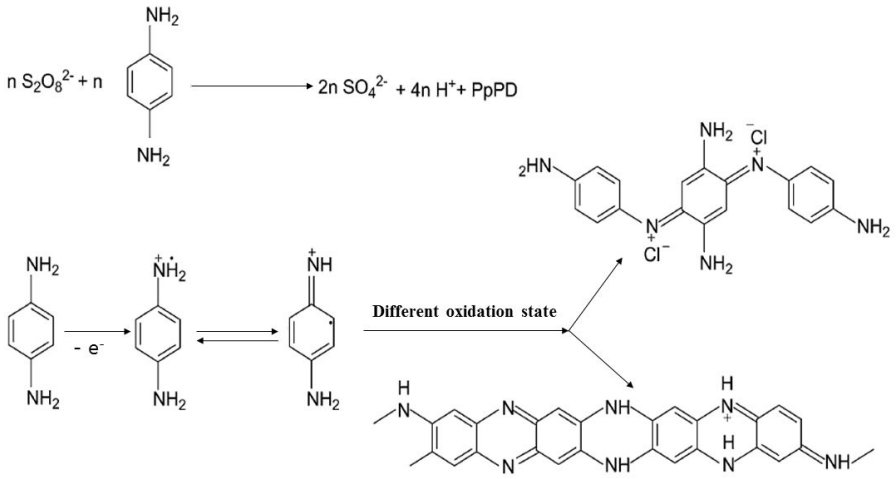

Scheme 2. Probable mechanism of the *p*PD monomer polymerization by different oxidation states.

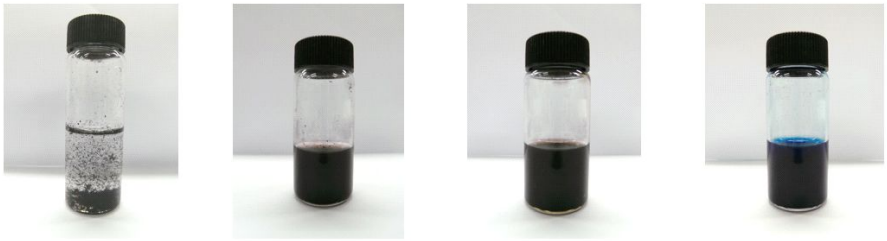

(a) **(b)** **(c)** **(d)**

Scheme 3. The visual image of (a) Pristine MWCNTs, (b) MWCNTs@P*p*PD in pH 7.0, (c) MWCNTs@P*p*PD in pH 3.5, (d) MWCNTs@P*p*PD-PB.

The chemical components of the as-synthesized samples were investigated by FTIR. Fig. 1 shows the FTIR spectra of MWCNTs, MWCNTs@P*p*PD, and MWCNTs@P*p*PD-PB. The spectrum of MWCNTs exhibits a weaker absorption at 3440 cm^{-1} and other minor peaks (a). After the polymerization of *p*PD on the surface of MWCNTs, the characteristic absorption peaks of P*p*PD were observed. The board absorption peaks located at 3444 cm^{-1} and the shoulder peak located at 3216 cm^{-1} could be because of the N–H stretching vibration of the –NH group in MWCNTs@P*p*PD (b). Furthermore, in another broad adsorption peak assigned approximately from 1650 to 1300 cm^{-1}, the two strong peaks located at 1606 and 1545 cm^{-1} can be attributed to the C=N and C=C stretching vibration of the phenazine ring structure, respectively. The other peak located at 1494 cm^{-1} corresponds to the stretching of the benzene ring. The two small peak at 1262 and 1208 cm^{-1} are assigned to the imine C=N stretching vibration of the benzoid and quinoid imine units (–C=N–), proving that P*p*PD was successfully polymerized on MWCNTs [43]. Compared to the spectrum of MWCNTs@P*p*PD, the MWCNTs@P*p*PD-PB nanocomposite showed a strong absorption peak at 2083 cm^{-1}. This peak is attributed to the C≡N stretching absorption band in the [Fe^{2+}–CN–Fe^{3+}] structure of PB. An absorption peak at 502 cm^{-1} was also observed, because of the formation of [Fe^{2+}–CN–Fe^{3+}] structure. Both the peaks indicate the presence of PB [60]. Finally, the shoulder peak in the spectrum of MWCNTs@P*p*PD disappeared in that of MWCNTs@P*p*PD-PB, indicating that the N–H bond of P*p*PD rarely exist.

Fig. 2 shows the XRD patterns of the pristine MWCNTs, P*p*PD,

MWCNTs@P*p*PD, and MWCNTs@P*p*PD-PB nanocomposites. The peaks centered at 26° and 43° correspond to the (0 0 2) and (1 0 0) reflection of graphite from the MWCNTs, respectively (Fig. 2(a)) [61]. The XRD pattern of the P*p*PD nanofibers (Fig. 2(b)) shows four big sharp peaks and eight minor peaks between 2θ = 8–30° [40]. Fig. 2(c) shows the XRD pattern of MWCNTs@P*p*PD, indicating the overlap between the XRD patterns of MWCNTs and P*p*PD nanofibers. It means that the coating of P*p*PD did not destroy the crystal structure of graphite from MWCNTs. Compared to the XRD pattern of the MWCNTs@P*p*PD, the peaks of MWCNTs@P*p*PD-PB are observed at 2 θ values of 17.5°, 24.8°, 35.3°, 39.6°, 50.6°, 54.0° and 57.1° corresponding to the (2 0 0), (2 2 0), (4 0 0), (4 2 0), (4 4 0), (6 0 0), and (6 2 0) reflections, respectively [62]. All the reflections can be indexed as a pure face-centered-cubic phase of $Fe_4[Fe(CN)_6]_3$, clearly demonstrating the successful synthesis of PB on the modified MWCNTs [63]. All the reflections can be indexed as a pure face-centered-cubic phase of $Fe_4[Fe(CN)_6]_3$, according to the standard values for the bulk cubic Prussian blue (JCPDS card no. 73-0687).

The average diameter of PBNPs was calculated using the Scherrer formula [64]:

$$t = \frac{0.9\lambda}{B\cos\theta_B}$$

where t is the crystal size, λ is the wavelength of the X-ray, and *B* is the line width, which is usually measured at the half-maximum intensity from the strong diffraction line ((2 0 0) diffraction line).

Moreover, θ_B is the Bragg angle of the reflection. The average diameter of the PBNPs was ~15.4 nm, calculated by the Scherrer formula. This size is analogous to the diameter of the PBNPs determined from the TEM images.

The morphologies and sizes of the as-synthesized nanocomposites are shown in Fig. 3. The TEM image of the pristine MWCNTs (Fig. 3(a)) shows the average diameter of 10.3 nm. The modified MWCNTs (Fig. 3(b)) coated with P*p*PD on the MWCNTs have the average diameter of 18.5 nm. It is wider than the pristine MWCNTs, which shows approximately 4 nm extent that can be conformed by the TEM image of the same magnification. Figs. 3(c) and 3(d) show typical MWCNTs@P*p*PD-PB nanocomposites synthesized under optimized conditions at different magnifications. As shown, the average diameter of PBNPs was measured at 30.7 nm as a mean of random 9 particles, with a cubic morphology.

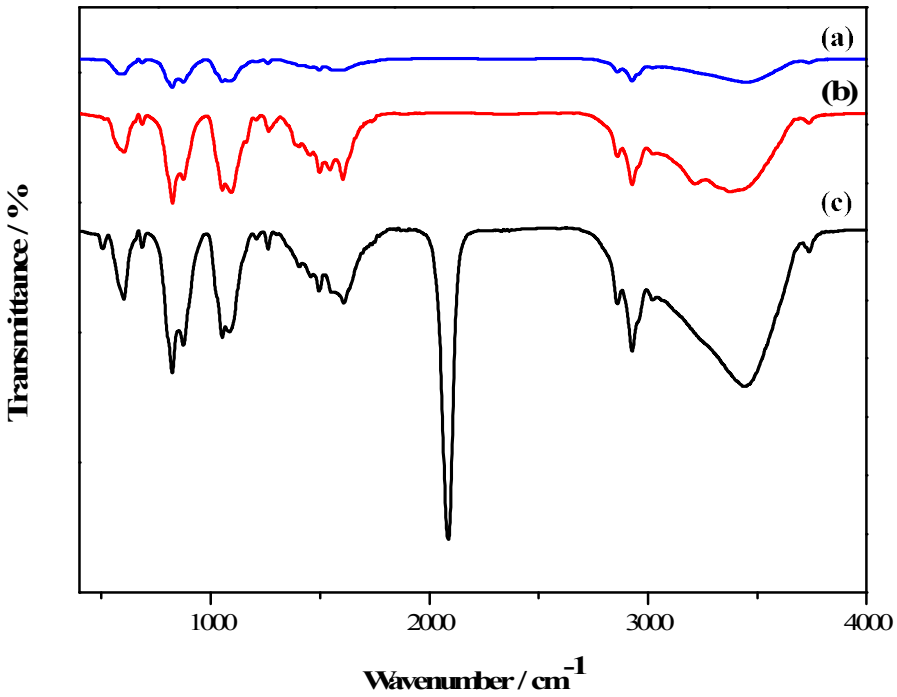

Figure 1. FTIR spectra of (a) MWCNTs, (b) MWCNTs@P*p*PD, and (c) MWCNTs@P*p*PD-PB nanocomposites.

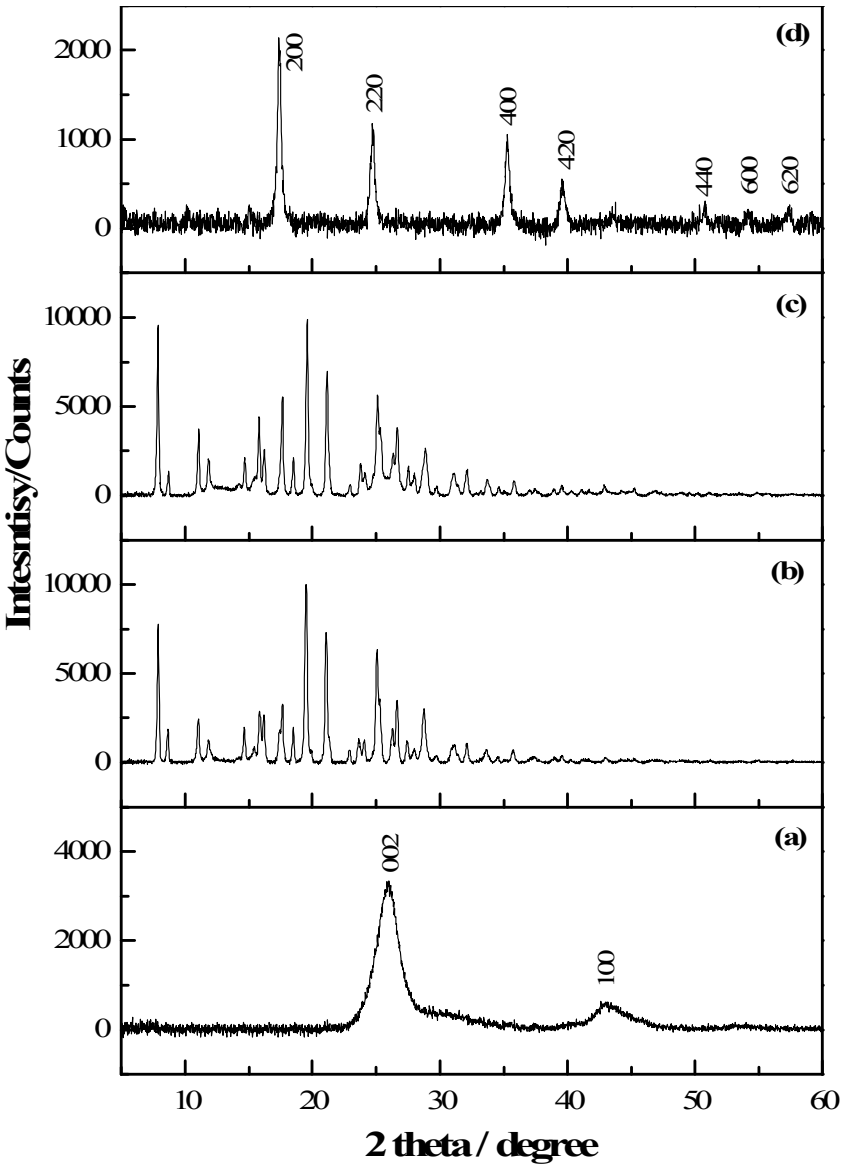

Figure 2. XRD patterns of (a) MWCNTs, (b) P*p*PD nanofibers, (c) MWCNTs@P*p*PD, and (d) MWCNTs@P*p*PD-PB nanocomposites.

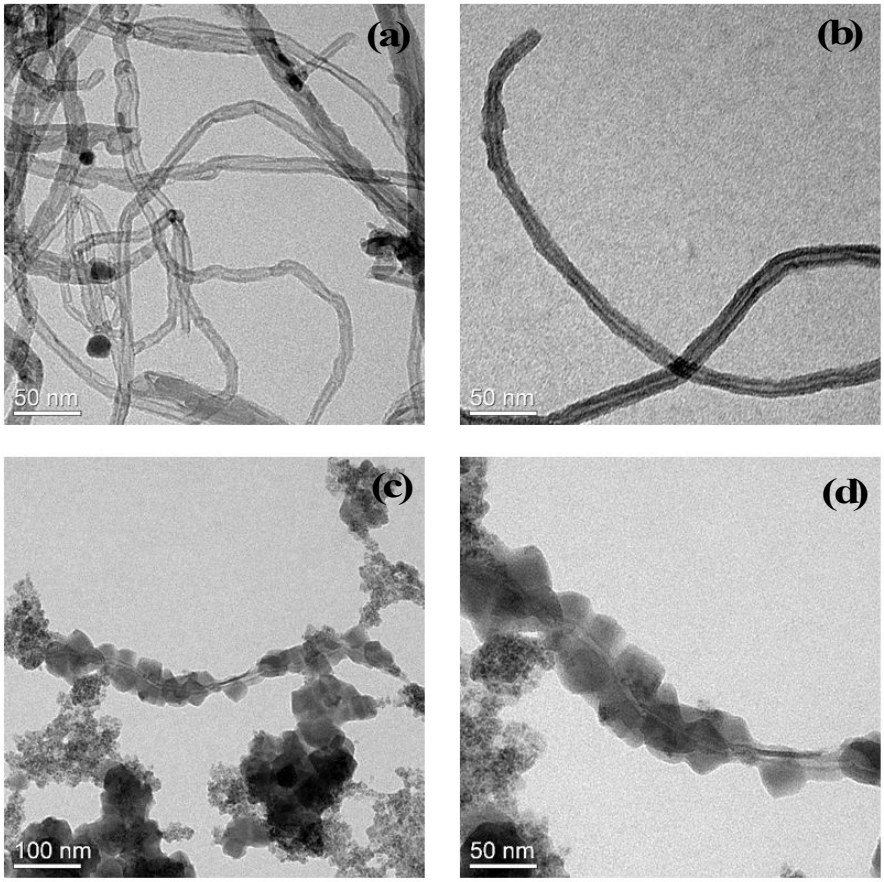

Figure 3. TEM images of (a) MWCNTs, (b) MWCNTs@P*p*PD, (c-d) MWCNTs@P*p*PD-PB nanocomposites at different magnifications.

3.2. Electrochemical impedance spectroscopy (EIS) characterization

Electrochemical impedance spectroscopy (EIS) provides information on the impedance changes of the electrode surface during the modification process. An archetypal impedance spectrum has a semicircle portion at higher frequencies corresponding to the electron-transfer-limited process and a linear portion at the lower frequency is attributable to a diffusion-limited electron transfer. The inset in Fig. 4 is the Randles equivalent circuit model used for fitting the measurement data, where R_s is electrolyte resistance, C_{dl} double layer capacitance, R_{ct} electron transfer resistance, and Z_w Warburg impedance. As mentioned earlier, the electron transfer resistance (R_{ct}) represents the electron-transfer-limited process at the electrode/electrolyte interface and is equal to the semicircle diameter in the Nyquist diagrams. It is measured in a background solution, containing 5 mM $[Fe(CN)_6]^{3-/4-}$ solution containing 0.1 M KCl in the frequency range from 10 mHz to 100 kHz at 0.19 V (vs. Ag/AgCl). Fig. 4 shows the impedance spectra represented as the Nyquist plots (Z′ vs Z") for (a) bare GCE, (b) GCE/PB, (c) GCE/MWCNTs, (d) GCE/MWCNTs@P*p*PD, and (e) GCE/MWCNTs@P*p*PD-PB. The R_{ct} of the bare GCE is 127.14 Ω with an almost straight tail line. While MWCNTs were cast on the GCE, the R_{ct} decreased to 42.66 Ω, indicating that the MWCNTs could prompt the charge transfer. Furthermore, when the GCE electrode surface was coated with PBNPs the R_{ct} value increased considerably to

421.79 Ω, indicating that the PBNPs on the GCE obstructed the electron transfer of the electrochemical process at the electrode surface. After the MWCNTs@P*p*PD dropped over the GCE, the diameter of the high frequency semicircle significantly reduced to 9.06 Ω as a R_{ct} value, indicating that *p*PD polymer may play an important role in accelerating the electron transfer process. The R_{ct} value of MWCNTs@P*p*PD-PB is 42.43 Ω, which is greater than the value of the already synthesized MWCNTs@P*p*PD, indicating that PB interrupted the electron transfer.

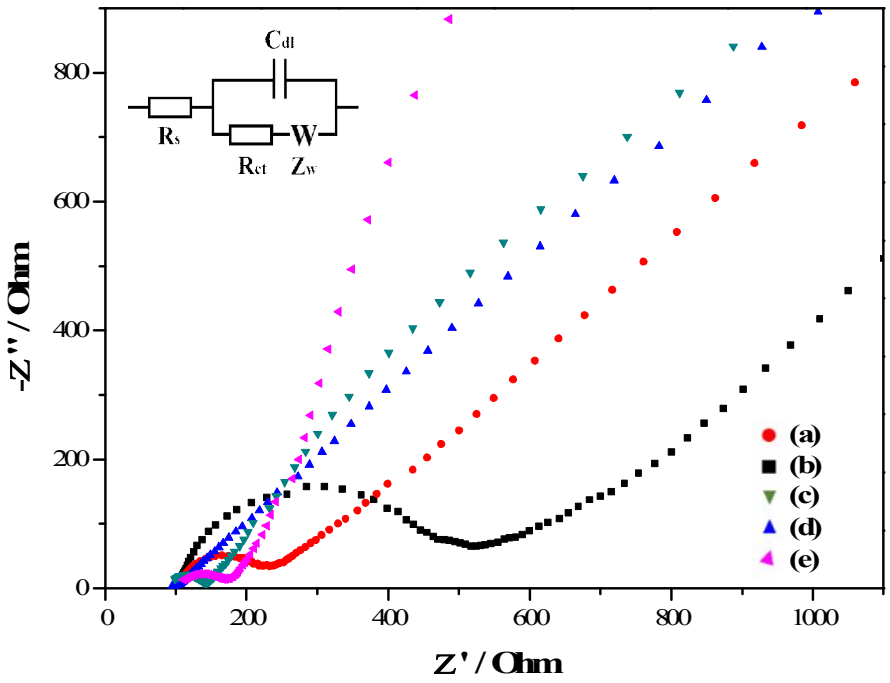

Figure 4. Nyquist plots of (a) bare GCE, (b) GCE/PB, (c) GCE/MWCNTs, (d) GCE/MWCNTs@P*p*PD and (e) GCE/MWCNTs@P*p*PD-PB in 0.1 M KCl solution containing 5 mM $[Fe(CN)_6]^{3-}$ and 5 mM $[Fe(CN)6]^{4-}$.

3.3 Voltammetric behaviors of H_2O_2 at GCE/MWCNTs@PpPD-PB

To demonstrate the synergistic effect of the MWCNTs@P*p*PD-PB nanocomposites, cyclic voltammetry (CV) was used for characterizing the electrochemical properties of the composites modified GCE in N_2 saturated 0.1 M KCl (pH 2.7) aqueous solution at a scan rate of 50 mV s^{-1}. Fig. 5 shows the CVs of the bare GCE, GCE/MWCNTs, GCE/MWCNTs@P*p*PD, GCE/MWCNTs-PB, and GCE/MWCNTs@P*p*PD-PB in the absence of H_2O_2. The reversible pair of redox peaks are observed at MWCNTs-PB (Fig. 5(d)) and MWCNTs@P*p*PD-PB modified GCE (Fig. 5(e)), whereas no redox pair peaks were observed for the bare GCE (Fig. 5(a)), GCE/MWCNTs (Fig. 5(b)) and GCE/MWCNTs@P*p*PD (Fig. 5(c)).

A pair of well-developed redox waves corresponded to the inter-conversion between PB and PW. Between the observed redox peaks, the peak current of MWCNTs@P*p*PD-PB modified GCE is much larger than its MWCNTs-PB modified GCE, probably because of high electrical conductivity of the coated *p*PD polymer on the MWCNTs. After adding 5 mM H_2O_2, the CVs of the bare GCE (Fig. 6(a)), GCE/MWCNTs (Fig. 6(b)) and GCE/MWCNTs@PpPD (Fig. 6(c)) did not change. Meanwhile, the CVs of the MWCNTs-PB (Fig. 6(d)) and MWCNTs@PpPD-PB modified GCE (Fig. 6(e)) show that the reduction peak significantly increased, but the oxidation peak decreased slightly,

which are different from the CVs in Fig. 5. These results indicate the presence of PBNPs on the modified GCE. PB is well known for excellent electrocatalytic activity towards the reduction of H_2O_2.

According to an earlier study [65], this electrocatalytic process is a two steps process shown by the following equation:

$$KFe^{III}[Fe^{II}(CN)_6]\ (PB) + K^+ + e^- \rightarrow K_2Fe^{II}[Fe^{II}(CN)_6]\ (PW) \quad (1)$$

$$2K_2Fe^{II}[Fe^{II}(CN)_6]\ (PW) + H_2O_2 + 2H^+ \rightarrow 2KFe^{III}[Fe^{II}(CN)_6]\ (PB) + 2H_2O + 2K^+ \quad (2)$$

First, PB is reduced to PW at the surface of the electrode. Then, the PW is reoxidized to PB in the presence of H_2O_2, which is simultaneously reduced with water, i. e., the current value of H_2O_2 reduction significantly increased, because of the role of the electrocatalyst PB, as confirmed by CV.

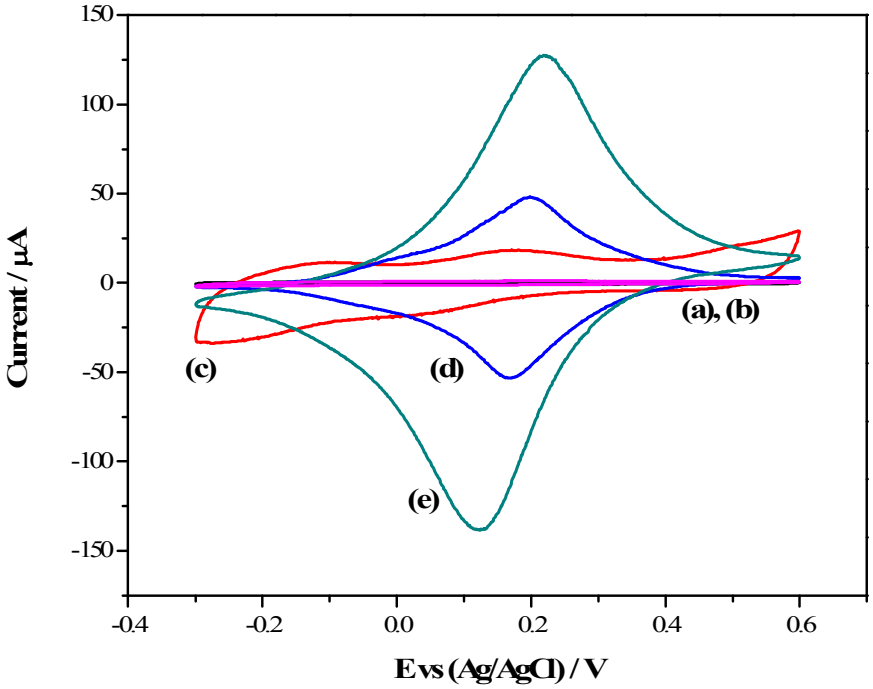

Figure 5. CVs of (a) bare GCE, (b) GCE/MWCNTs, (c) GCE/MWCNTs@P*p*PD, (d) GCE/MWCNTs-PB, and (e) GCE/MWCNTs@P*p*PD-PB in the absence of H_2O_2 from −0.3 to 0.6 V in 0.1 M KCl solution (pH 2.7) at scan rate of 50 mV s^{-1}.

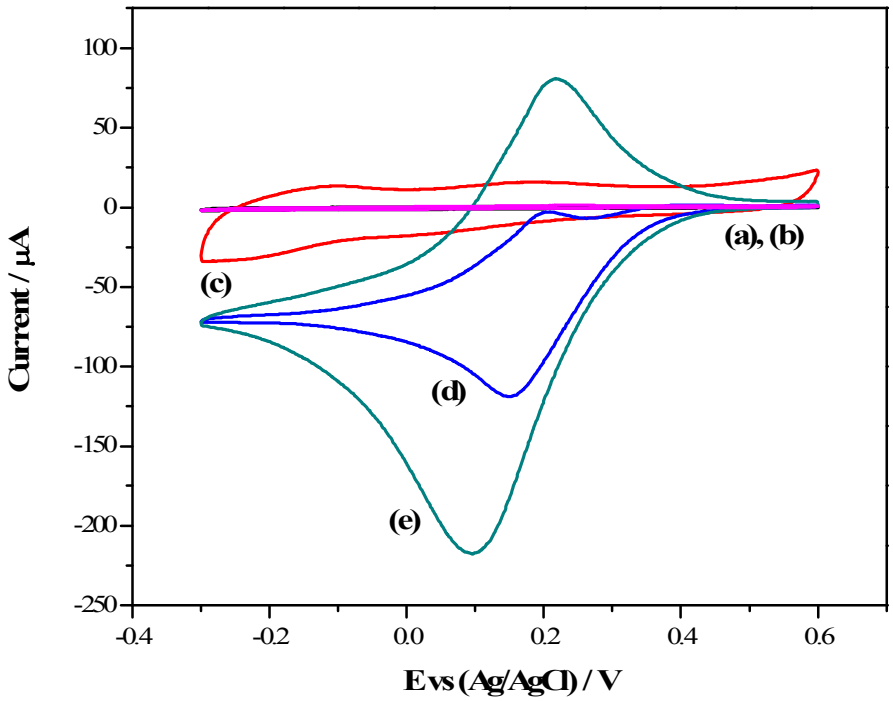

Figure 6. CVs of (a) bare GCE, (b) GCE/MWCNTs, (c) GCE/MWCNTs@P*p*PD, (d) GCE/MWCNTs-PB, and (e) GCE/MWCNTs@P*p*PD-PB in 5 mM H_2O_2 from −0.3 to 0.6 V in 0.1 M KCl solution (pH 2.7) at scan rate of 50 mV s^{-1}.

Figs. 7(A) and 7(B) show the CVs of GCE/MWCNTs-PB and GCE/MWCNTs@P*p*PD-PB in N_2-saturated 0.1 M KCl (pH 2.7) at different concentrations of H_2O_2. The cathodic peak current value increases with increasing concentration of H_2O_2. because of the PB. Moreover, Fig. 8 shows that the reduction current of the MWCNTs@P*p*PD-PB modified GCE is about twice as high as that of the MWCNTs-PB modified GCE. The more specific comparison of these modified electrodes can be observed by the amperometry.

The correlation between the current and the scan rate is shown in Fig. 9. The electrochemical effect of the scan rate on the electrocatalytic H_2O_2 cathodic current was investigated to evaluate the kinetics of the electrochemical performance of the as-synthesized MWCNTs nanocomposites. The cathodic peak currents increased linearly in proportion to the square root of the scan rate with a correlation coefficient of 0.9978 (inset in Fig. 9) as the scan rate was increased from 10 to 200 mV s^{-1}. This result signifies that the process of electrocatalytic reaction is diffusion-controlled.

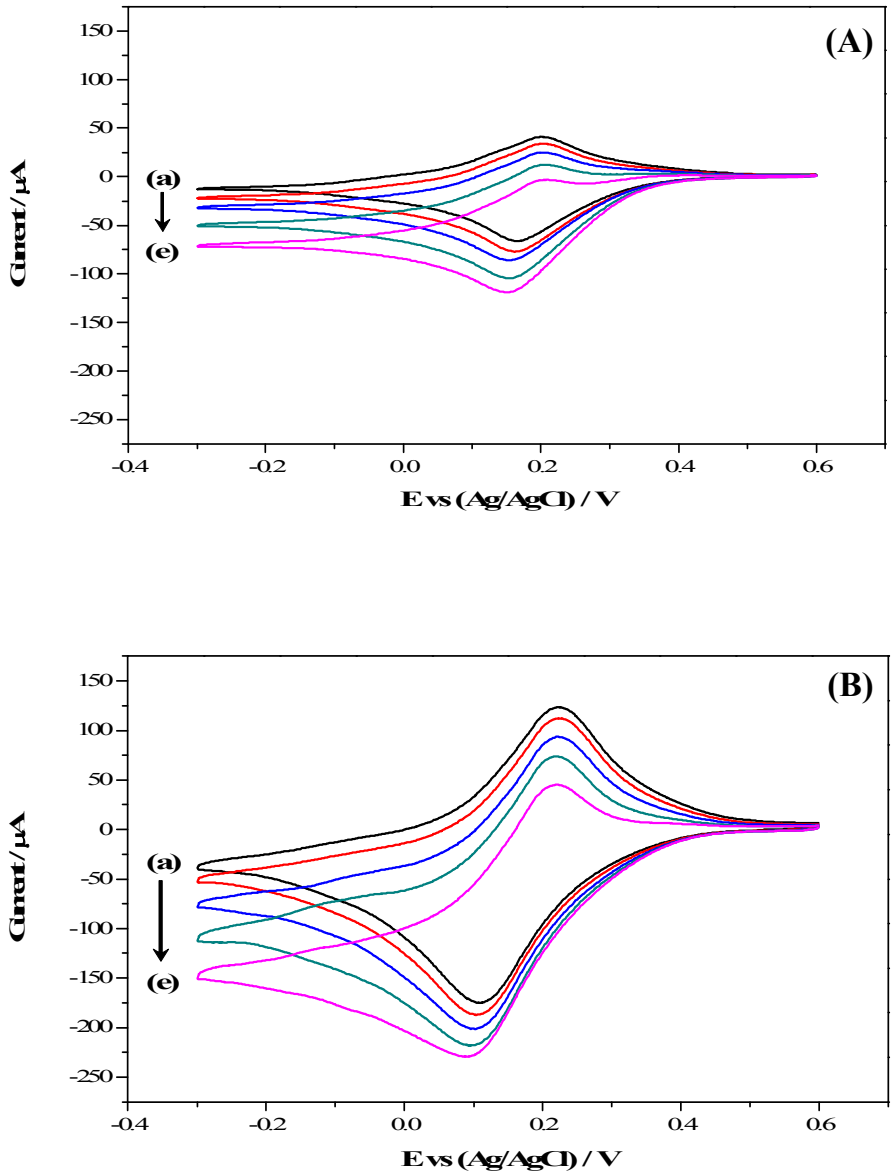

Figure 7. CVs of **(A)** GCE/MWCNTs-PB and **(B)** GCE/MWCNTs@P*p*PD-PB in N_2-saturated 0.1M KCl aqueous solution (pH 2.7) in the presence of H_2O_2 with different concentrations (from (a) to (e) : 1, 2, 3, 4, and 5 mM) at a scan rate of 50 mV s^{-1}.

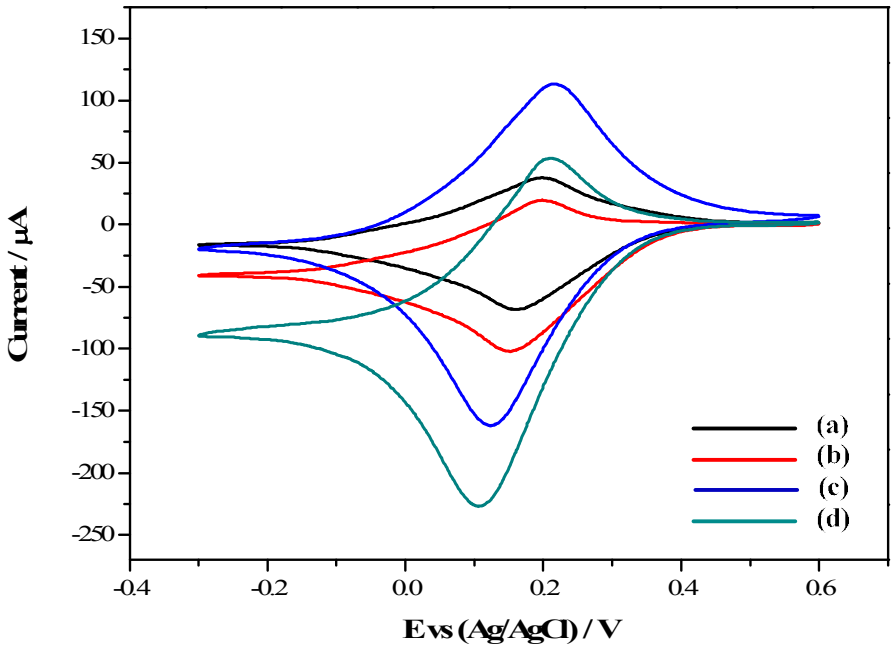

Figure 8. CVs of 1 mM H_2O_2 on (a) GCE/MWCNTs-PB, (c) GCE/MWCNTs@P*p*PD-PB and 5 mM H_2O_2 on (b) GCE/MWCNTs-PB, (d) GCE/MWCNTs@P*p*PD-PB from −0.3 to 0.6 V in 0.1 M KCl solution (pH 2.7) at scan rate of 50 mV s^{-1}.

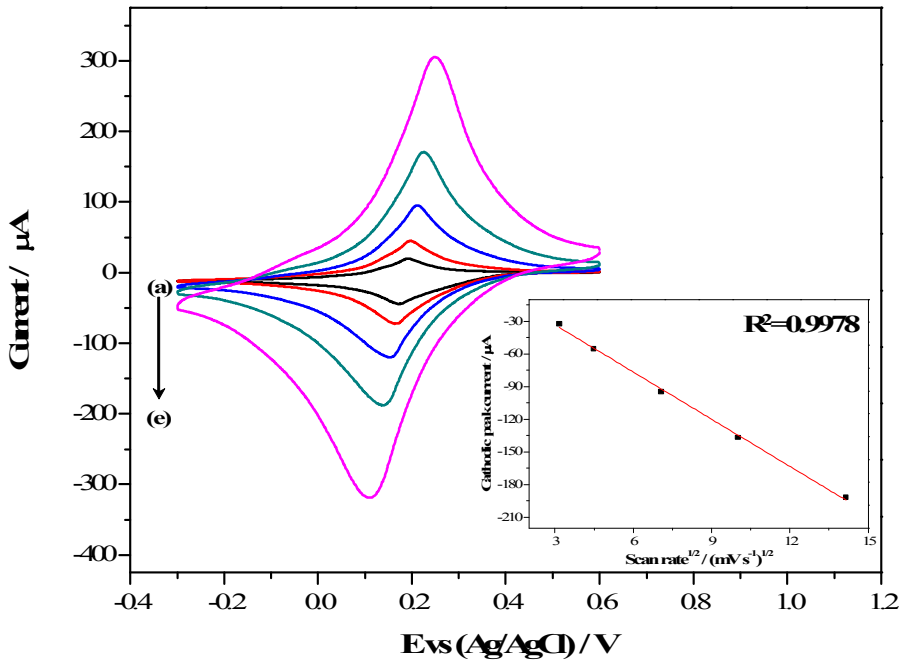

Figure 9. CVs of MWCNTs@P*p*PD-PB nanocomposite modified glassy carbon electrode in N_2-saturated 0.1M KCl aqueous solution (pH 2.7) in the presence of 1 mM H_2O_2 at different scan rates (from (a) to (e) : 10, 20, 50, 100, 200 mV s^{-1}).

3.4 Amperometric response of H_2O_2 at GCE/MWCNTs-PB and GCE/MWCNTs@PpPD-PB

Fig. 10(A) shows the comparative amperometric response of GCE/MWCNTs-PB (Fig. 10(A) (a)) and GCE/MWCNTs@P*p*PD-PB (Fig. 10(A) (b)) for successive sensing of H_2O_2 into stirred N_2-saturated 0.1 M KCl (pH 2.7) aqueous solution at an applied potential of +0.15 V (vs. Ag/AgCl). The reduction current value showed a rapid response to the subsequent addition of H_2O_2 and quickly reached to the 95% steady-state current, which was less than 2 s. In the MWCNTs-PB modified GCE and the MWCNTs@P*p*PD-PB modified GCE, the current for both increases with the addition of H_2O_2, and the latter current value is greater than the former. The fast and large amperometric response is ascribed to the synergistic effect of MWCNTs, P*p*PD, and PB. First, the synergistic effect of MWCNTs and PB was attributed to the formation the MWCNTs. They provide a three-dimensional network of electrical conductivity, thus improving the electrical and ionic transport capacity [66]. Simultaneously, the reduction currents of H_2O_2 improved because of the electrocatalytic activity of PB [67]. Despite this, the amperometric response was unstable with the addition of H_2O_2 because of the weak interaction between the MWCNTs and the PBNPs. To solve this problem, the MWCNTs were effectively coated by P*p*PD reliably, and strongly attached to the PBNPs. The P*p*PD is electrically conductive polymer, and it increases the electron transfer efficiency. As

a result, it increases the reduction currents of H_2O_2. Therefore, the modified electrode composed of the MWCNTs, P*p*PD, and PB showed a better response to the addition of H_2O_2.

Fig. 10(B) shows the calibration curve of the reduction peak currents vs. the concentration of H_2O_2. As shown, it presents the linear response region of MWCNTs-PB (Fig. 10(B) (a)) and MWCNTs@P*p*PD-PB (Fig. 10(B) (b)). The result of MWCNTs-PB modified GCE is similar to that of a previously reported study [68]. Fig. 10(B) (b) shows a linear response range from 0.005 mM to 2.225 mM with a correlation coefficient of 0.9992, and the sensitivity of the sensor was 583.6 μA $mM^{-1}cm^{-2}$, which was much higher than that of a previous study estimated from GCE/MWCNTs-PB and GCE/MWCNTs/Ppy/PB. Moreover, the limit of detection of GCE/MWCNTs@P*p*PD-PB was calculated as 0.95 μM with a signal-to-noise ratio of 3. Table 1 summarizes the electrochemical characteristics of various modified electrodes containing PB for sensing H_2O_2, indicating that GCE/MWCNTs@P*p*PD-PB has a high sensitivity and a wide linear range in comparison to those of other reported modified electrodes, proving improved electrical conductivity and good stability.

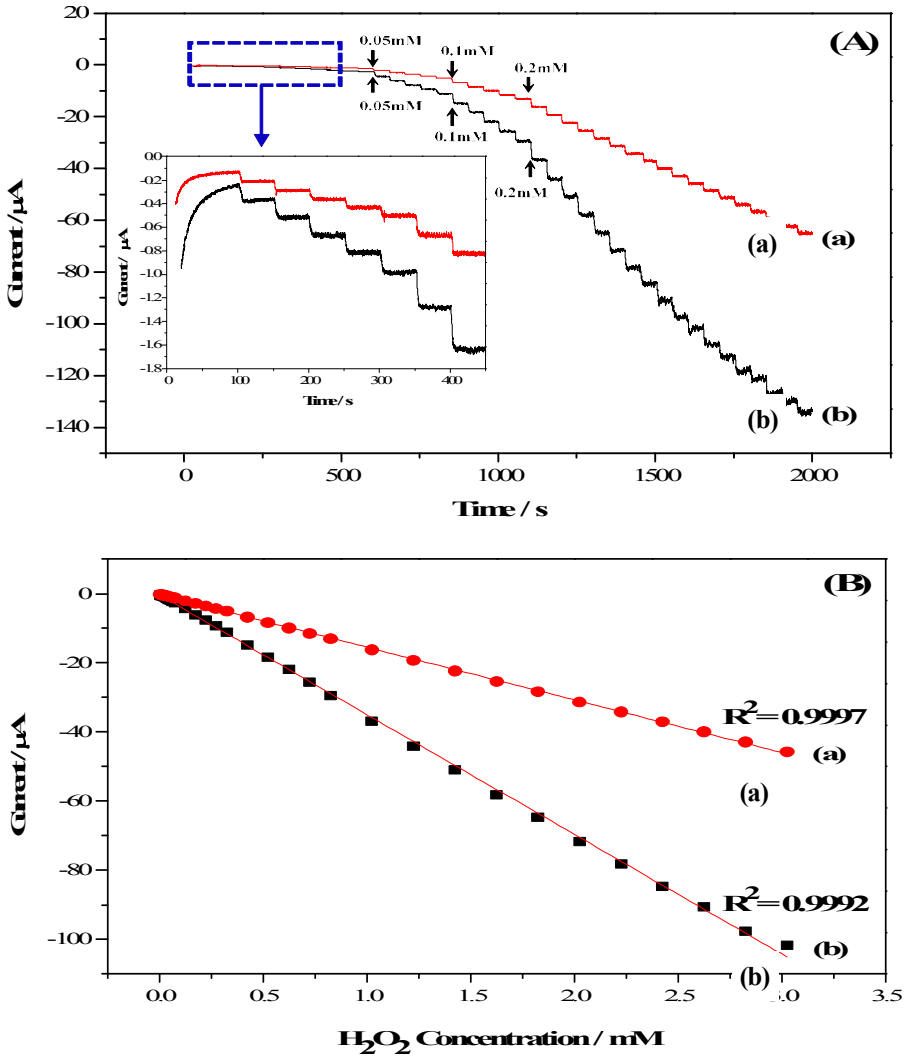

Figure 10. (A) Amperometric response of the (a) MWCNTs-PB and (b) MWCNTs@P*p*PD-PB nanocomposite modified glassy carbon electrode to successive injection of H_2O_2 in 0.1 M KCl aqueous solution (pH 2.7) under stirring. Applied potential: +0.15 V. **(B)** Calibration curve of the reduction peak current (a) MWCNTs-PB and (b) MWCNTs@P*p*PD-PB nanocomposite modified glassy carbon electrode versus concentration of H_2O_2.

Table 1. Electrochemical characteristics of various PB contained electrodes toward hydrogen peroxide.

Electrode	Linear range (mM)	Sensitivity ($\mu A/(mMcm^2)$)	Limit of detection (μM)	Applied Potential (V)	Reference
GCE/MWNTs/PANI/PB	0.0008-2	526.43	0.005	0	[69]
GCE/graphene/PB	0.02-0.2	196.6	1.9	-0.05	[70]
GCE/MWCNT/PB	0.01-0.4	153.7	0.567	0	[68]
GCE/SWNTs/PB	0.5-27.5	12.02	0.01	-0.1	[71]
GCE/$[PB@PtNPs/PCNTs]_2$	2.5×10^{-4}-1.5	850	0.15	+0.1	[72]
GE/PBMPs/Nafion	0.0021-0.14	138.6	1	-0.05	[21]
GCE/MWCNT/Ppy/PB	0.004-0.517	345	0.08	-0.3	[31]
GCE/MWCNTs@P*p*PD-PB	**0.005-2.225**	**583.6**	**0.95**	**0.15**	**This work**

3.5 Selectivity, reproducibility, and stability of the H_2O_2 sensor

An amperometric measurement was performed to assess the selectivity of the as-synthesized sensor. The interference study was needed for biological application [73]. Fig. 11 shows that the current generated in the presence of 0.1 mM interfering substances, such as citric acid, ascorbic acid, and L-cysteine, could be ignored relative to the current attributed solely to 0.1 mM H_2O_2 in N_2-saturated 0.1 M KCl solution (pH 2.7) at an applied potential of 0.15 V, indicating that this sensor possessed an excellent anti-interference capacity. The reproducibility was investigated by the CV experiments on five modified electrodes under the same condition, showing excellent performance as evidenced by a relative standard deviation (RSD) of 2.5%.

Fig. 12 shows the stability examined by monitoring the current response in 1 mM H_2O_2 solution after effectively cycling the modified electrode. After 50 cycles, the reduction of the electrode signal is only 2.6%, and after 50 additional cycles, the loss of signal reached only 2.9%. To determine the life span of the prepared sensor, the as-synthesized electrodes were stored in a refrigerator at 4 °C, and the electrode signal decreased to only 97.1% of its original peak current in 1 mM H_2O_2 after 20 days.

Therefore, the MWCNTs@P*p*PD-PB on the GCE showed excellent selectivity, reproducibility, and stability. The current response becomes stable in less than 2 s, which indicates the rapid response of the MWCNTs@P*p*PD-PB on the GCE towards H_2O_2.

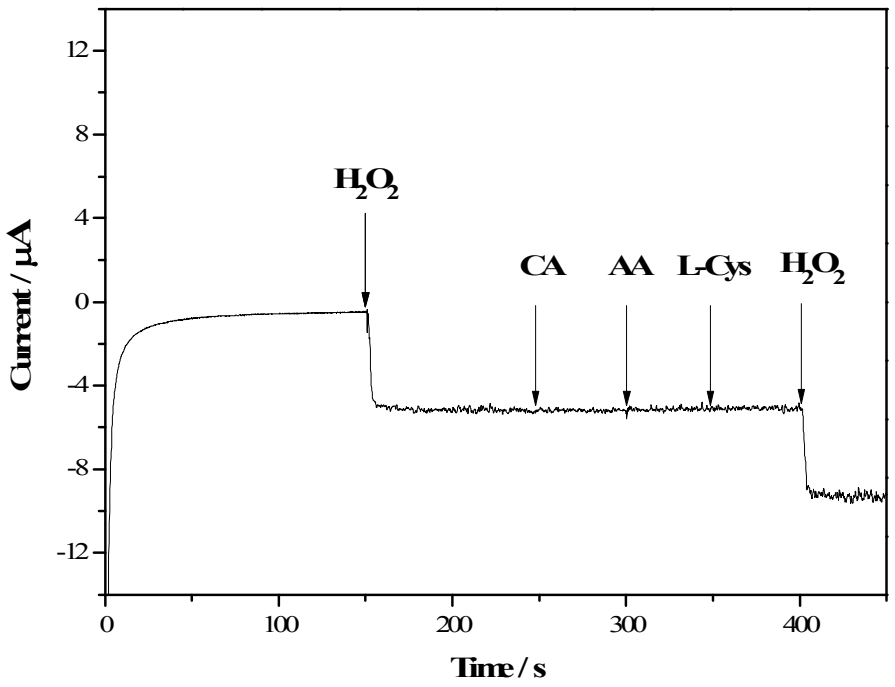

Figure 11. Interference-free behavior of the MWCNTs@P*p*PD-PB nanocomposite modified GCE by the amperometric trace that was recorded in N_2-saturated 0.1 M KCl solution (pH 2.7) under stirring. Injection of 0.1 mM H_2O_2, citric acid (CA), ascorbic acid (AA), and L-Cysteine (L-Cys). Applied potential: +0.15 V.

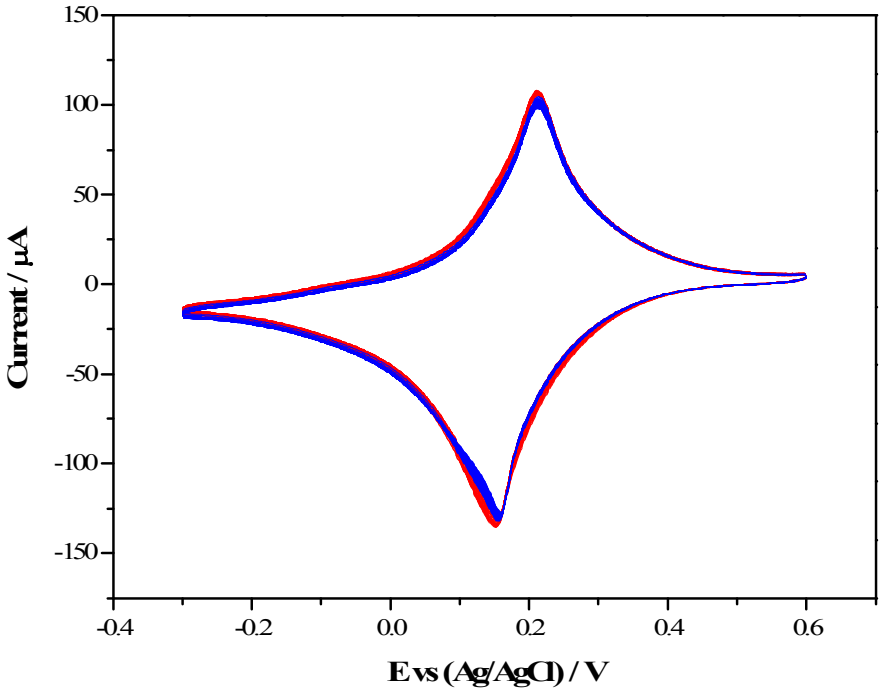

Figure 12. CVs of GCE/MWCNTs@P*p*PD-PB in 1 mM H_2O_2 and 0.1 M KCl aqueous solution (pH 2.7) at 50 mV s^{-1} for 100 cycles.

3.6 Real sample analysis

The performance of MWCNTs@P*p*PD-PB nanocomposites on the GCE was analyzed by applying it to the determination of H_2O_2 present in disinfectant. Using amperometry measurement to obtain the response of the real sample, the experiment was conducted under the same conditions as the conventional amperometry experimental conditions. The exact H_2O_2 concentration in the real sample was measured using the standard addition method. The concentrations obtained by stepwise increasing the concentration and the RSD are listed in Table 2. The recoveries of H_2O_2 were found to be in the range 95-100%, indicating that the modified electrode is suitable for real sample analyses.

Table 2. Electroanalytical values obtained from the determination of H_2O_2 in disinfectant using i-t curve in 0.1 M KCl solution (pH 2.7) by MWCNTs@P*p*PD-PB composites modified GCE.

Experiment No.	Spiked (μM)	Found (μM)	Recovery (%)	R.S.D. (%)
1	49.45	49.43	99.95	0.16
2	147.78	142.96	96.74	0.51
3	244.35	232.91	95.32	1.54

[a] R.S.D.(%) calculated form five separate experiments

4. Conclusions

In this study, an approach for simple fabrication of sensitive nonenzymatic electrochemical detection of H_2O_2 is described based on MWCNTs@P*p*PD-PB nanocomposites. The MWCNTs@P*p*PD was easily synthesized without structural destruction of MWCNTs by P*p*PD coating. The P*p*PD not only serves to ensure a good dispersion of MWCNTs in the water, but also increases the reduction currents of H_2O_2. The PBNPs were adhered strongly and uniformly on the as-synthesized MWCNTs, because of the P*p*PD. They exhibited an excellent electrocatalytic activity for the reduction of H_2O_2. Therefore, this modified electrode indicates the increasing reduction peak currents value with a rapid current. Furthermore, it showed a good linear range, high sensitivity, low detection limit, good reproducibility, and better stability. The MWCNTs@P*p*PD-PB modified glassy carbon electrode can be applied successfully to detect H_2O_2 in real samples as nonenzymatic sensors.

5. References

[1] F. Herren, P. Fischer, A. Ludi, W. Haelg, Neutron diffraction study of Prussian Blue, $Fe_4[Fe(CN)_6]^3$.xH2O. Location of water molecules and long-range magnetic order, Inorg. Chem. 19 (1980) 956–959.

[2] L. Wang, S. Guo, X. Hu, S. Dong, Layer-by-layer assembly of carbon nanotubes and Prussian blue nanoparticles: A potential tool for biosensing devices, Colloids Surfaces A Physicochem. Eng. Asp. 317 (2008) 394–399.

[3] A.A. Karyakin, Prussian Blue and Its Analogues: Electrochemistry and Analytical Applications, Electroanalysis. 13 (2001) 813–819.

[4] D. Zhang, K. Wang, D.C. Sun, X.H. Xia, H.-Y. Chen, Ultrathin Layers of Densely Packed Prussian Blue Nanoclusters Prepared from a Ferricyanide Solution, Chem. Mater. 15 (2003) 4163–4165.

[5] D. Zhang, K. Wang, D. Sun, X. Xia, H. Chen, Potentiodynamic deposition of Prussian blue from a solution containing single component of ferricyanide and its mechanism investigation, J. Solid State Electrochem. 7 (2003) 561–566.

[6] D. Ellis, M. Eckhoff, V.D. Neff, Electrochromism in the mixed-valence hexacyanides. 1. Voltammetric and spectral studies of the oxidation and reduction of thin films of Prussian blue, J. Phys. Chem. 85 (1981) 1225–1231.

[7] R.J. Mortimer, Five Color Electrochromicity Using Prussian Blue and Nafion/Methyl Viologen Layered Films, J. Electrochem. Soc. 138 (1991) 633.

[8] P. Somani, A.. Mandale, S. Radhakrishnan, Study and development of conducting polymer-based electrochromic display devices, Acta Mater. 48 (2000) 2859-2871.

[9] D. Weidinger, D.J. Brown, J.C. Owrutsky, Transient absorption studies of vibrational relaxation and photophysics of Prussian blue and ruthenium purple nanoparticles., J. Chem. Phys. 134 (2011) 124510.

[10] M. Pyrasch, B. Tieke, Electro- and Photoresponsive Films of Prussian Blue Prepared upon Multiple Sequential Adsorption, Langmuir. 17 (2001) 7706-7709.

[11] C. Mingotaud, C. Lafuente, J. Amiell, P. Delhaes, Ferromagnetic Langmuir-Blodgett Film Based on Prussian Blue, Langmuir. 15 (1999) 289-292.

[12] P. Zhou, D. Xue, H. Luo, X. Chen, Fabrication, Structure, and Magnetic Properties of Highly Ordered Prussian Blue Nanowire Arrays, Nano Lett. 2 (2002) 845-847.

[13] F. Ricci, G. Palleschi, Y. Yigzaw, L. Gorton, T. Ruzgas, A. Karyakin, Investigation of the Effect of Different Glassy Carbon Materials on the Performance of Prussian Blue Based Sensors for Hydrogen Peroxide, Electroanalysis. 15 (2003) 175-182.

[14] F. Ricci, G. Palleschi, Sensor and biosensor preparation, optimisation and applications of Prussian Blue modified electrodes., Biosens. Bioelectron. 21 (2005) 389-407.

[15] D. Moscone, D. D'Ottavi, D. Compagnone, G. Palleschi, A. Amine, Construction and Analytical Characterization of Prussian Blue-Based

Carbon Paste Electrodes and Their Assembly as Oxidase Enzyme Sensors, Anal. Chem. 73 (2001) 2529–2535.

[16] J.-H. Yang, N. Myoung, H.-G. Hong, Facile and controllable synthesis of Prussian blue on chitosan-functionalized graphene nanosheets for the electrochemical detection of hydrogen peroxide, Electrochim. Acta. 81 (2012) 37–43.

[17] Q. Sheng, D. Zhang, Q. Wu, J. Zheng, H. Tang, Electrodeposition of Prussian blue nanoparticles on polyaniline coated halloysite nanotubes for nonenzymatic hydrogen peroxide sensing, Anal. Methods. 7 (2015) 6896–6903.

[18] S.-Q. Liu, J.-J. Xu, H.-Y. Chen, Electrochemical behavior of nanosized Prussian blue self-assembled on Au electrode surface, Electrochem. Commun. 4 (2002) 421–425.

[19] D. Zhang, K. Zhang, Y.L. Yao, X.H. Xia, H.Y. Chen, Multilayer assembly of Prussian blue nanoclusters and enzyme-immobilized poly(toluidine blue) films and its application in glucose biosensor construction., Langmuir. 20 (2004) 7303–7.

[20] V.D. Neff, Electrochemical Oxidation and Reduction of Thin Films of Prussian Blue, J. Electrochem. Soc. 125 (1978) 886.

[21] B. Haghighi, H. Hamidi, L. Gorton, Electrochemical behavior and application of Prussian blue nanoparticle modified graphite electrode, Sensors Actuators B Chem. 147 (2010) 270–276.

[22] A.A. Karyakin, E.E. Karyakina, L. Gorton, The electrocatalytic activity of Prussian blue in hydrogen peroxide reduction studied using

a wall-jet electrode with continuous flow, J. Electroanal. Chem. 456 (1998) 97−104.

[23] A.A. Karyakin, E.E. Karyakina, L. Gorton, Amperometric Biosensor for Glutamate Using Prussian Blue-Based "Artificial Peroxidase"as a Transducer for Hydrogen Peroxide, Anal. Chem. 72 (2000) 1720−1723.

[24] R. Garjonyte, A. Malinauskas, Glucose biosensor based on glucose oxidase immobilized in electropolymerized polypyrrole and poly(o-phenylenediamine) films on a Prussian Blue-modified electrode, Sensors Actuators B Chem. 63 (2000) 122−128.

[25] Q. Chi, S. Dong, Amperometric biosensors based on the immobilization of oxidases in a Prussian blue film by electrochemical codeposition, Anal. Chim. Acta. 310 (1995) 429−436.

[26] J. Zeng, W. Wei, X. Liu, Y. Wang, G. Luo, A simple method to fabricate a Prussian Blue nanoparticles/carbon nanotubes/poly(1,2-diaminobenzene) based glucose biosensor, Microchim. Acta. 160 (2007) 261−267.

[27] Q. Zhang, L. Zhang, J. Li, Fabrication and electrochemical study of monodisperse and size controlled Prussian blue nanoparticles protected by biocompatible polymer, Electrochim. Acta. 53 (2008) 3050−3055.

[28] N.A. Pchelintsev, A. Vakurov, P.A. Millner, Simultaneous deposition of Prussian Blue and creation of an electrostatic surface for rapid biosensor construction, Sensors Actuators B Chem. 138 (2009) 461−466.

[29] S. Han, Y. Chen, R. Pang, P. Wan, M. Fan, Fabrication of Prussian Blue/Multiwalled Carbon Nanotubes/Glass Carbon Electrode through Sequential Deposition, Ind. Eng. Chem. Res. 46 (2007) 6847−6851.

[30] X.-W. Liu, Z.-J. Yao, Y.-F. Wang, X.-W. Wei, Graphene oxide sheet-prussian blue nanocomposites: green synthesis and their extraordinary electrochemical properties., Colloids Surf. B. Biointerfaces. 81 (2010) 508–12.

[31] E. Jin, X. Bian, X. Lu, C. Wang, Fabrication of multiwalled carbon nanotubes/polypyrrole/Prussian blue ternary composite nanofibers and their application for enzymeless hydrogen peroxide detection, J. Mater. Sci. 47 (2012) 4326–4331.

[32] Z. Wang, G. Shi, J. Xia, Y. Xia, F. Zhang, L. Xia, et al., Facile preparation of a Pt/Prussian blue/graphene composite and its application as an enhanced catalyst for methanol oxidation, Electrochim. Acta. 121 (2014) 245–252.

[33] P. Wang, Y. Yuan, X. Wang, G. Zhu, Renewable three-dimensional Prussian blue modified carbon ceramic electrode, J. Electroanal. Chem. 493 (2000) 130–134.

[34] S. Vaucher, M. Li, S. Mann, Synthesis of Prussian Blue Nanoparticles and Nanocrystal Superlattices in Reverse Microemulsions, Angew. Chemie Int. Ed. 39 (2000) 1793–1796.

[35] X. Zhu, X. Niu, H. Zhao, M. Lan, Doping ionic liquid into Prussian blue-multiwalled carbon nanotubes modified screen-printed electrode to enhance the nonenzymatic H2O2 sensing performance, Sensors Actuators B Chem. 195 (2014) 274–280.

[36] L. Zhang, Z. Song, Q. Zhang, X. Jia, H. Zhang, S. Xin, Enhancement of the Electrochemical Performance of Prussian Blue

Modified Electrode via Ionic Liquid Treatment, Electroanalysis. 21 (2009) 1835–1841.

[37] A. Cabrera-García, A. Vidal-Moya, Á. Bernabeu, J. Sánchez-González, E. Fernández, P. Botella, Gd-Si oxide mesoporous nanoparticles with pre-formed morphology prepared from a Prussian blue analogue template., Dalton Trans. 44 (2015) 14034–41.

[38] Y. Guari, J. Larionova, K. Molvinger, B. Folch, C. Guérin, Magnetic water-soluble cyano-bridged metal coordination nano-polymers., Chem. Commun. (Camb). (2006) 2613–5.

[39] F.S. Kim, G. Ren, S.A. Jenekhe, One-Dimensional Nanostructures of π-Conjugated Molecular Systems: Assembly, Properties, and Applications from Photovoltaics, Sensors, and Nanophotonics to Nanoelectronics, Chem. Mater. 23 (2011) 682–732.

[40] S. Yang, F. Liao, Poly(p-phenylenediamine) nanofibers having conjugated structures, a novel, simple and highly selective fluorescent probe for l-cysteine, Synth. Met. 162 (2012) 1343–1347.

[41] P. Magdziarz, P. Bober, M. Trchová, Z. Morávková, M. Bláha, J. Proke , et al., Conducting composites prepared by the reduction of silver ions with poly(p -phenylenediamine), Polym. Int. 64 (2015) 496 –504.

[42] J.L. Boehme, D.S.K. Mudigonda, J.P. Ferraris, Electrochromic Properties of Laminate Devices Fabricated from Polyaniline, Poly(ethylenedioxythiophene), and Poly(N -methylpyrrole), Chem. Mater. 13 (2001) 4469–4472.

[43] X.-G. Li, M.-R. Huang, W. Duan, Y.-L. Yang, Novel Multifunctional Polymers from Aromatic Diamines by Oxidative Polymerizations, Chem. Rev. 102 (2002) 2925−3030.

[44] J. Xu, P. Yao, X. Li, F. He, Synthesis and characterization of water-soluble and conducting sulfonated polyaniline/para-phenylenediamine-functionalized multi-walled carbon nanotubes nano-composite, Mater. Sci. Eng. B. 151 (2008) 210−219.

[45] I. Amer, D.A. Young, Chemically oxidative polymerization of aromatic diamines: The first use of aluminium-triflate as a co-catalyst, Polymer (Guildf). 54 (2013) 505−512.

[46] Y. Haldorai, W.S. Lyoo, J.-J. Shim, Poly(aniline-co-p-phenylenediamine)/MWCNT nanocomposites via in situ microemulsion: synthesis and characterization, Colloid Polym. Sci. 287 (2009) 1273−1280.

[47] X. Han, S. Liu, Y. Yuan, Y. Wang, L. Hu, Experimental study on synthesis and microstructure of poly (p-phenylenediamine)/graphene oxide/Au and its performance in supercapacitor, J. Alloys Compd. 543 (2012) 200−205.

[48] Y. Haldorai, P.Q. Long, S.K. Noh, W.S. Lyoo, J.-J. Shim, Ultrasonically assisted in situ emulsion polymerization: a facile approach to prepare conducting copolymer/silica nanocomposites, Polym. Adv. Technol. 22 (2011) 781−787.

[49] S. Iijima, Helical microtubules of graphitic carbon, Nature. 354 (1991) 56−58.

[50] F. Zhao, X. Wu, M. Wang, Y. Liu, L. Gao, S. Dong, Electrochemical and bioelectrochemistry properties of room-temperature

ionic liquids and carbon composite materials., Anal. Chem. 76 (2004) 4960−7.

[51] P.M. Ajayan, Nanotubes from Carbon, Chem. Rev. 99 (1999) 1787−1800.

[52] Y.-P. Sun, K. Fu, Y. Lin, W. Huang, Functionalized Carbon Nanotubes: Properties and Applications, Acc. Chem. Res. 35 (2002) 1096−1104.

[53] M. Baghayeri, E. Nazarzadeh Zare, M. Mansour Lakouraj, A simple hydrogen peroxide biosensor based on a novel electro-magnetic poly(p-phenylenediamine)@Fe_3O_4 nanocomposite., Biosens. Bioelectron. 55 (2014) 259−65.

[54] S. Hanaoka, J.-M. Lin, M. Yamada, Chemiluminescent flow sensor for H2O2 based on the decomposition of H2O2 catalyzed by cobalt(II)-ethanolamine complex immobilized on resin, Anal. Chim. Acta. 426 (2001) 57−64.

[55] Y. Li, A. Townshend, Evaluation of the adsorptive immobilisation of horseradish peroxidase on PTFE tubing in flow systems for hydrogen peroxide determination using fluorescence detection, Anal. Chim. Acta. 359 (1998) 149−156.

[56] C. Matsubara, N. Kawamoto, K. Takamura, Oxo[5, 10, 15, 20-tetra(4-pyridyl)porphyrinato]titanium(IV): an ultra-high sensitivity spectrophotometric reagent for hydrogen peroxide, Analyst. 117 (1992) 1781.

[57] A. Chen, S. Chatterjee, Nanomaterials based electrochemical sensors for biomedical applications., Chem. Soc. Rev. 42 (2013) 5425–38.

[58] F. Liu, L. Wang, Q. Yin, B. Jiang, Optimization of thermoelectric figure of merit in poly(p-phenylenediamine)/exfoliated graphene nanosheets composites, RSC Adv. 4 (2014) 51558–51568.

[59] Z. Song, R. Yuan, Y. Chai, B. Yin, P. Fu, J. Wang, Multilayer structured amperometric immunosensor based on gold nanoparticles and Prussian blue nanoparticles/nanocomposite functionalized interface, Electrochim. Acta. 55 (2010) 1778-1784.

[60] E. Reguera, J. Fernández-Bertrán, J. Balmaseda, The existence of ferrous ferricyanide, Transit. Met. Chem. 24 (n.d.) 648–654.

[61] Y. Jiang, Y. Lu, L. Zhang, L. Liu, Y. Dai, W. Wang, Preparation and characterization of silver nanoparticles immobilized on multi-walled carbon nanotubes by poly(dopamine) functionalization, J. Nanoparticle Res. 14 (2012) 938.

[62] X. Wu, M. Cao, C. Hu, X. He, Sonochemical Synthesis of Prussian Blue Nanocubes from a Single-Source Precursor, Cryst. Growth Des. 6 (2006) 26–28.

[63] ICDD, International Centre for Diffraction Data (ICDD), Newtown Square, n.d.

[64] B.D. Cullity & S.R. Stock, Elements of X-Ray Diffraction (3rd Edition), Prentice Hall. (2001) 664 pages.

[65] P.A. Fiorito, V.R. Gonçales, E.A. Ponzio, S.I.C. de Torresi, Synthesis, characterization and immobilization of Prussian blue nanoparticles. A potential tool for biosensing devices., Chem. Commun. (Camb). (2005) 366–8.

[66] M. Zhang, W. Gorski, Electrochemical sensing platform based on the carbon nanotubes/redox mediators-biopolymer system., J. Am. Chem. Soc. 127 (2005) 2058–9.

[67] J. Li, J.-D. Qiu, J.-J. Xu, H.-Y. Chen, X.-H. Xia, The Synergistic Effect of Prussian-Blue-Grafted Carbon Nanotube/Poly(4-vinylpyridine) Composites for Amperometric Sensing, Adv. Funct. Mater. 17 (2007) 1574–1580.

[68] J. Zhai, Y. Zhai, D. Wen, S. Dong, Prussian Blue/Multiwalled Carbon Nanotube Hybrids: Synthesis, Assembly and Electrochemical Behavior, Electroanalysis. 21 (2009) 2207–2212.

[69] Y. Zou, L. Sun, F. Xu, Prussian Blue electrodeposited on MWNTs-PANI hybrid composites for H(2)O(2) detection., Talanta. 72 (2007) 437–42.

[70] E. Jin, X. Lu, L. Cui, D. Chao, C. Wang, Fabrication of graphene/prussian blue composite nanosheets and their electrocatalytic reduction of H_2O_2, Electrochim. Acta. 55 (2010) 7230–7234.

[71] W. Zhang, L. Wang, N. Zhang, G. Wang, B. Fang, Functionalization of Single-Walled Carbon Nanotubes with Cubic Prussian Blue and Its Application for Amperometric Sensing, Electroanalysis. 21 (2009) 2325 –2330.

[72] J. Zhang, J. Li, F. Yang, B. Zhang, X. Yang, Preparation of Prussian blue@Pt nanoparticles/carbon nanotubes composite material for efficient determination of H_2O_2, Sensors Actuators B Chem. 143 (2009) 373−380.

[73] J.-H. Lee, H.-G. Hong, Nonenzymatic electrochemical sensing of hydrogen peroxide based on a polyaniline-MnO2 nanofiber-modified glassy carbon electrode, J. Appl. Electrochem. 45 (2015) 1153−1162.

국문요약

파라-페닐렌다이아민이 입혀진 다중벽 탄소나노튜브에 프러시안 블루 나노복합물을 통한 과산화수소의 전기화학적 검출

본 연구에서 다중벽 탄소나노튜브(Multi-walled carbon nanotubes, MWCNTs)에 폴리파라페닐렌다이아민(Poly(*p*-phenylenediamine), P*p*PD)을 쉽게 코팅하여 프러시안블루(Prussian Blue, PB)을 접합시킨 나노복합물인 다중벽 탄소나노튜브@폴리파라페닐렌다이아민-프러시안블루(MWCNTs@P*p*PD-PB)가 전기화학적 과산화수소 검출에 효과적으로 응용 될 수 있음을 보여주었다.

폴리파라페닐렌다이아민층이 다중벽 탄소나노튜브를 물에 잘 분산되도록 할 뿐만 아니라, 다중벽 탄소나노튜브 표면에 프러시안블루(PB) 나노입자가 형성되고 고정되는 것을 돕는다. 또한, 폴리파라페닐렌다이아민이 전도성을 띄고 있는 고분자로서 다중벽 탄소나노튜브의 높은 전자전도성과 안정성을 증가시켜준다. 이러한 기능과 함께 프러시안블루의 과산화수소에 대한 선택성과 촉매능력을 결합시켜 과산화수소 검출에 대한 시너지 효과를 확인할 수 있었다.

합성된 다중벽 탄소나노튜브@폴리파라페닐렌다이아민-프러시안블루 나노복합물의 구조적 특성과 화학적 구성은 푸리에 변환 적외분광법(Fourier transform infrared spectroscopy, FT-IR), 투과전자현미경(Transmission electron microscopy, TEM), X-선 회절법(X-ray diffraction, XRD) 등을 이용해 분석하였다. 다중벽 탄소나노튜브@폴리파라페닐렌다이아민-프러시안블루 나노복합물 분산액을 유리탄소전극

(Glassy carbon electrode, GCE)의 표면에 떨어뜨려 말리는 방법인 드롭-캐스팅(Drop-casting) 을 이용하여 수정된 다중벽 탄소나노튜브@폴리파라페닐렌다이아민-프러시안블루 유리탄소전극(GCE/MWCNTs@P*p*PD-PB)을 제작하였다.

수정된 유리탄소전극의 과산화수소검출에 대한 비효소적 전기화학 센서의 전기화학적 활동을 알아보고자 전기화학적 임피던스 분석법(Electrochemical impedance spectroscopy, EIS), 순환전압전류법(Cyclic voltammetry, CV), 시간전류법(Amperometry) 등의 분석방법을 사용하였다. 연구 결과, 수정된 전극이 pH 2.7 수용액에서 과산화수소 환원에 대해 우수한 전기화학적 촉매 특성을 나타내었다. 이러한 과산화수소 센서는 넓은 선형구간 0.005-2.225 mM, 높은 감도 583.6 μA mM^{-1} cm^{-2}, 낮은 검출한계 0.95 μM (S/N=3)로 기존의 프러시안블루를 응용한 전극에 비해 우수한 결과를 보여주었다.

본 연구에서는 다중벽 탄소나노튜브 지지체를 통한 안정된 프러시안 블루 나노복합물 합성이 간단하게 이루어지고, 저렴한 가격으로 과산화수소 검출에 우수한 센서로서 성능을 보여줄 수 있음을 확인할 수 있다. 또한, 폴리파라페닐렌다이아민의 다기능적 성질(자가중합, 흡착성, 친수성)을 통해 탄소나노튜브가 구조적 결함 없이 표면을 개질하도록 하는데 중요한 역할을 하고 있음을 확인할 수 있다. 이러한 합성법의 개발이 과산화수소의 전기화학적 검출에 대한 최적의 조건을 제시해주며, 이는 후속 전기화학센서 연구에 다양하게 응용될 수 있을 것으로 기대한다.

주요어: 과산화수소, 다중벽탄소나노튜브,
파라페닐렌다이아민, 프러시안블루,
시간전류법, 센서

학 번: 2014-20956